**THE EUROPEAN
PHYSICAL JOURNAL B**

Regular Article

2D Hexagonal SnTe monolayer: a quasi direct band gap semiconductor with strain sensitive electronic and optical properties

Negin Fatahi[1], D.M. Hoat[2,3,a], Amel Laref[4], Shorin Amirian[1], A.H. Reshak[5,6,7], and Mosayeb Naseri[1]

[1] Department of Physics, Kermanshah Branch, Islamic Azad University, Kermanshah, Iran
[2] Computational Laboratory for Advanced Materials and Structures, Advanced Institute of Materials Science, Ton Duc Thang University, Ho Chi Minh City, Vietnam
[3] Faculty of Applied Sciences, Ton Duc Thang University, Ho Chi Minh City, Vietnam
[4] Department, College of Science, King Saud University, Riyadh, Saudi Arabia
[5] Physics Department, College of Science, Basrah University, Basrah, Iraq
[6] Nanotechnology and Catalysis Research Center (NANOCAT), University of Malaya, Kuala Lumpur 50603, Malaysia
[7] Department of Instrumentation and Control Engineering, Faculty of Mechanical Engineering, CTU in Prague, Technicka 4, Prague 6 166 07, Czech Republic

Abstract. The stability and electronic and optical properties of two-dimensional (2D) **SnTe** monolayer has been systematically studied by using first-principles calculations based on density functional theory. Our computations demonstrate that the predicted 2D **SnTe** monolayer is a stable quasi-direct semiconductor. Also, analysis of its electronic property shows that the ground state of this monolayer is a quasi-direct semiconductor with a band gap of ~ 2.00. This band gap can be effectively modulated by external strains. Investigation of optical properties shows that monolayer **SnTe** exhibits significant absorption and reflectivity in the ultraviolet region of the electromagnetic spectrum.

1 Introduction

It is well-known that low-dimensional materials show rich physical and chemical properties as compared with their bulk (3D) counterpart [1,2]. Graphene is a two-dimensional (2D) allotrope of carbon with high density and an unusual combination of properties, such as high mechanical strength, hardness, and conductivity and adjustable electrical and superior optical and superficial properties. Graphene was discovered in 2004 [3], and, after this discovery, 2D monolayer materials were considered significant in the design of new optoelectronic devices [4–12]. In recent years, a variety of graphene-like materials such as phosphorene, silicene, germanium, arsenene, antimonene, and bismuthene have been fabricated and studied [13–20] and several excellent 2D nanostructures have been predicted theoretically and synthesized experimentally [20–33].

In this work, based on density functional theory (DFT) and using a first-principles calculation in this framework, we surveyed 2D nanoscale structure **SnTe**. DFT calculations have been widely employed to calculate and

predict materials properties [34,35]. As the first step, the ground state of the possible stable 2D **SnTe** monolayer was obtained. Afterward, cohesive energy calculations and phonon mode simulation were employed to prove the stability of the proposed monolayer. After the 2D **SnTe** monolayer stability was proved, the electronic and optical properties of the ground state of 2D **SnTe** monolayer were investigated by applying different approximations, i.e., the Perdew–Burke–Ernzerhof (PBE) exchange-correlation functional and the Heyd–Scuseria–Ernzerhof (HSE) hybrid functional approximation. Finally, by imposing biaxial strains on this monolayer, its electronic and optical properties were studied. By examining the physical properties of **SnTe**, it is found that this monolayer is a quasi-direct semiconductor with a strain-tunable band gap of ~ 1.25–2.00 eV. These calculated unique electronic and optical characteristics suggest that 2D **SnTe** monolayer is suitable for making new electronic devices.

This paper is organized as follows: details of the theoretical method are discussed in Section 2. Section 3 discusses optimization of ground state properties. The electronic and optical properties of the considered material are reported in Section 4. Finally, a summary is presented in the last section.
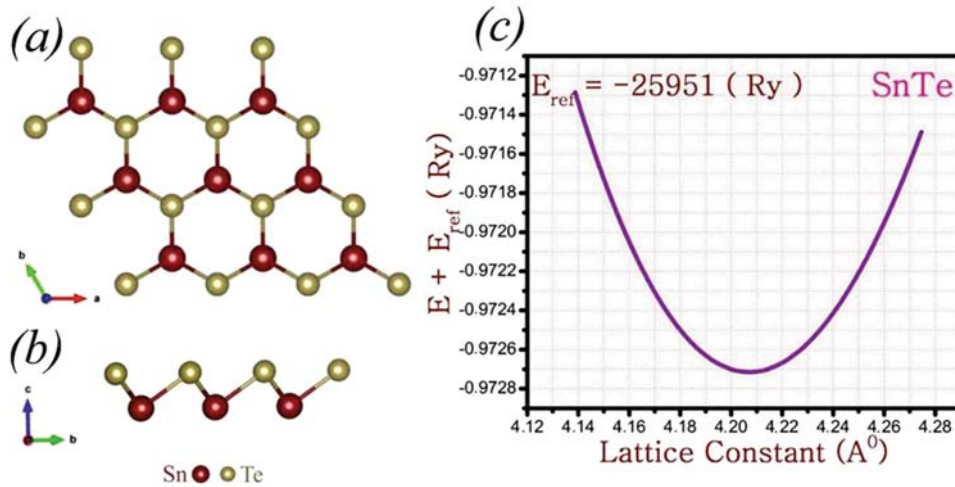
ᵃ e-mail: dominhhoat@tdtu.edu.vn

Fig. 1. Geometric atomic configurations of predicted **SnTe** structure: (a) top view and (b) side views. (c) Total energy diagram in terms of the lattice constant of a hexagonal unit cell of the **SnTe** structure.

2 Computational methodology

Geometry optimization and determination of the electronic and optical properties were done by using DFT based on first-principles calculations as implemented in the WIEN2k code [36]. For gaining a more accurate electronic band gap, two different theories were used: the generalized gradient approximation (GGA) PBE [37] approximation, which is a summarized GGA in the form of the PBE exchange-correlation functional, and the HSE hybrid functional theory (HSE06) [38]. In this calculation, the full potential linear augmented planewave plus local orbital (FPLAPW+lo) was applied to expand the Kohn–Sham wave functions. For the electronic and optical properties calculation, we used k-point meshes of $10 \times 10 \times 1$ and $20 \times 20 \times 1$ based on the Monkhorst–Pack scheme in the Brillouin zone [39]. In this computational method, we set the input parameters equal to $R_{\mathrm{MT}}K_{\max} = 7$, $G_{\max} = 14$ Ry, and $l\max = 10$. Also, a vacuum layer of 15 Å in the nonperiodic direction (z axis) was employed for avoiding interactions between neighboring layers.

To investigate the dynamic stability, computation of phonon modes was performed by running a first-principles calculation based on density functional perturbation theory, and the Quantum ESPRESSO package [40] was used for this purpose. In this package to treat the core electrons, the Martin–Troullier norm-conserving psedupotential [41] and an energy cutoff of 60 Ry were considered.

3 Properties of the optimized ground state

To theoretically study the physical properties of a crystal, one must first optimize the parameters such as lattice constants, the number of k-points, cutoff energy, and energy per volume.

As shown in Figure 1, there are two atoms (**Sn** and **Te**) in a hexagonal unit cell of the 2D **SnTe** monolayer. For optimizing the unit cells of the structures, first, atomic

coordinate optimizations and lattice optimization must be performed. Using the Birch–Murnaghan thermodynamic equation of state [42], lattice optimization was performed by calculating the total energies of the unit cells against their volumes as follows:

$$E(V) = E_0 + \frac{9 B_0 V_0}{16} \left\{ \left[\left(\frac{V_0}{V} \right)^{2/3} - 1 \right]^3 \acute{B_0} \right\}$$
$$+ \frac{9 B_0 V_0}{16} \left\{ \left[\left(\frac{V_0}{V} \right)^{2/3} - 1 \right]^2 \left[6a - 4 \left(\frac{V_0}{V} \right)^{2/3} \right] \right\},$$
(1)

where V_0 is the desired initial volume, V is the deformed volume, B_0 is the bulk modulus, and $\acute{B_0}$ is the derivative of the bulk modulus with respect to pressure. As is known, the minimum point on the E–V curve provides the lattice constant of the crystal cell in equilibrium. Therefore, with that in mind, the lattice constants of $a = b = 4.2071$ Å were obtained. In a **SnTe** monolayer supercell, two different planes exist: the Sn plane and Te plane; these are separated in the vertical distance equal to 1.678 Å. Structurally, each Sn is surrounded by three neighboring **Te** atoms and one **Te** atom is shared by three **Sn** atoms to form a hexagonal structure.

Now, we want to examine the stability of **SnTe** monolayer. To check the energetic stability of the material, its cohesive energies (E_{coh}) must be calculated. The cohesive energy for **SnTe** monolayer is defined as

$$E_{\mathrm{coh}} = \frac{n\, E_{\mathrm{Sn}}^{\mathrm{isolated}} + m\, E_{\mathrm{Te}}^{\mathrm{isolated}} - E_{SnTe}^{\mathrm{tot}}}{n + m}.$$

According to our calculations, $E_{\mathrm{SnTe}}^{\mathrm{tot}} = -25951.97268972$ is the total energy of the unit cell of the **SnTe** structure, $E_{\mathrm{Sn}}^{\mathrm{isolated}} = -12357.92893$ is the energy of a **Sn** atom, $E_{\mathrm{Te}}^{\mathrm{isolated}} = -13593.6040$ is the energy
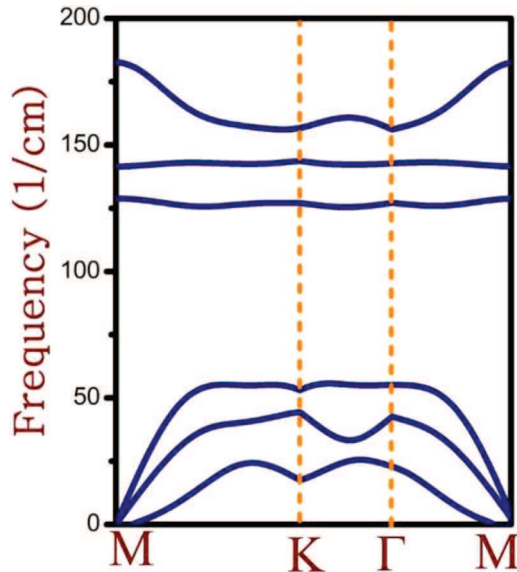
Fig. 2. Phonon dispersion in 2D **SnTe** monolayer.

Fig. 3. (Left) Band structures of SnTe obtained from PBE theory (green lines) and from the HSE06 approximation (red lines). (Right) Density of states of SnTe calculated by using the GGA PBE approximation.

of a **Te** atom, **n** is the number of **Sn** atoms, and **m** is the number of **Te** atoms in the unit cell. Finally, we obtained the cohesive energy for this 2D monolayer material equal to 3.00 eV, the positive feature of this parameter confirms its energetic stability.

Next, by using the Quantum ESPRESSO computational code, the dynamic stability of the 2D **SnTe** monolayer nanostructure was checked. For achieving this goal, its phonon dispersion diagram was drawn. As shown in Figure 2, phonon dispersion in 2D **SnTe** monolayer shows that the negative or imaginary phonon modes do not exist, indicating the dynamic stability of this nanostructure.

4 Electronic and optical properties

To apply the predicted **SnTe** monolayer in electronic applications, it is necessary to investigate its electronic properties. First, the band structure of the 2D **SnTe** monolayer was studied by using the PBE approximation, results are displayed in Figure 3. Our calculation using PBE theory shows that the 2D **SnTe** monolayer is a quasi-direct semiconductor with a band gap of ~2.00 eV and that both the valence band maximum (VBM) and the conduction band minimum (CBM) are located between Γ and M points. In most cases, PBE theory underestimates the band gap, so, for more accurate calculations, again we calculated the electronic band gap of 2D **SnTe** monolayer by using HSE06 and determined a modified band gap of ~2.60 eV.

One of the main factors determining the electronic properties of solids is the distribution of the energy of conduction band electrons and valence band electrons, the results of which can be presented as a curve of the density of states (DOS) versus the energy. The area under the DOS curve denotes the number of allowed states in which electrons can be present in that energy range. This quantity plays an important role in the analysis of the
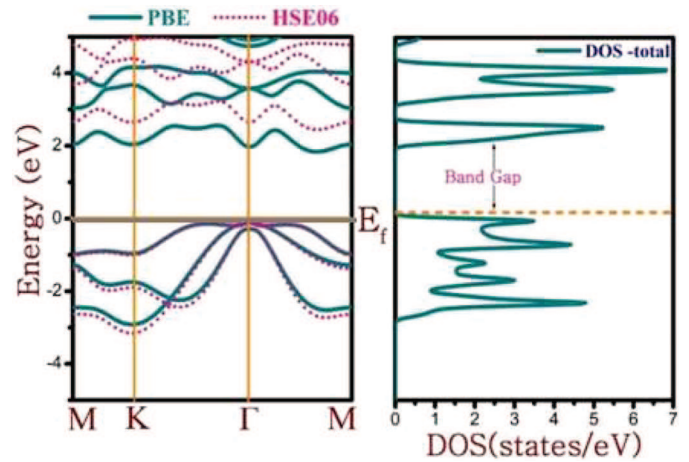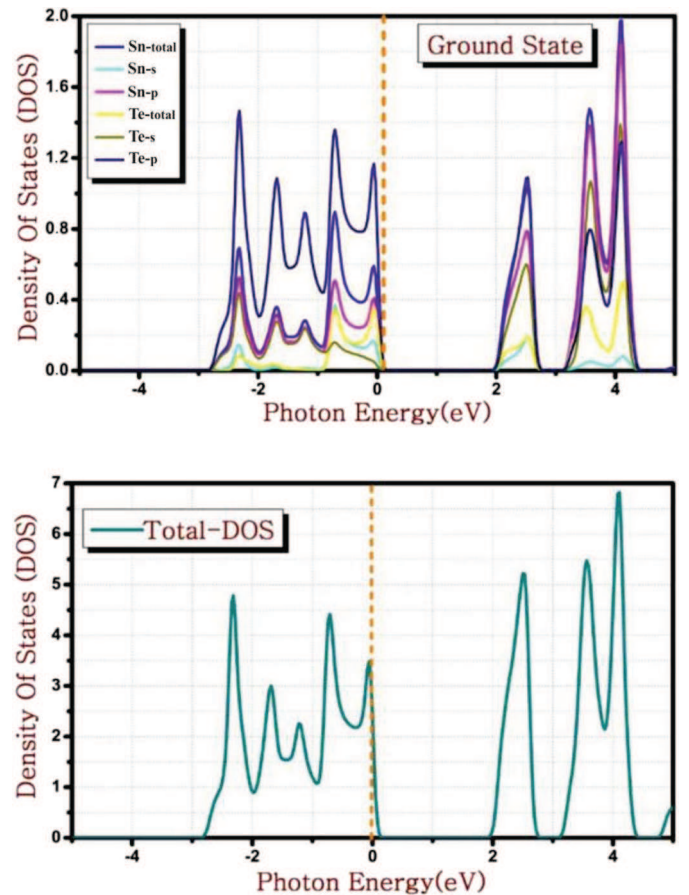

Fig. 4. SnTe electronic density of states obtained by using the GGA PBE approximation.

dielectric functions of solids. Also, theoretical values such as solid electron energy, the position of the fermion surfaces, and the probability of electron tunneling require accurate calculation of the DOS. The zero energy scale
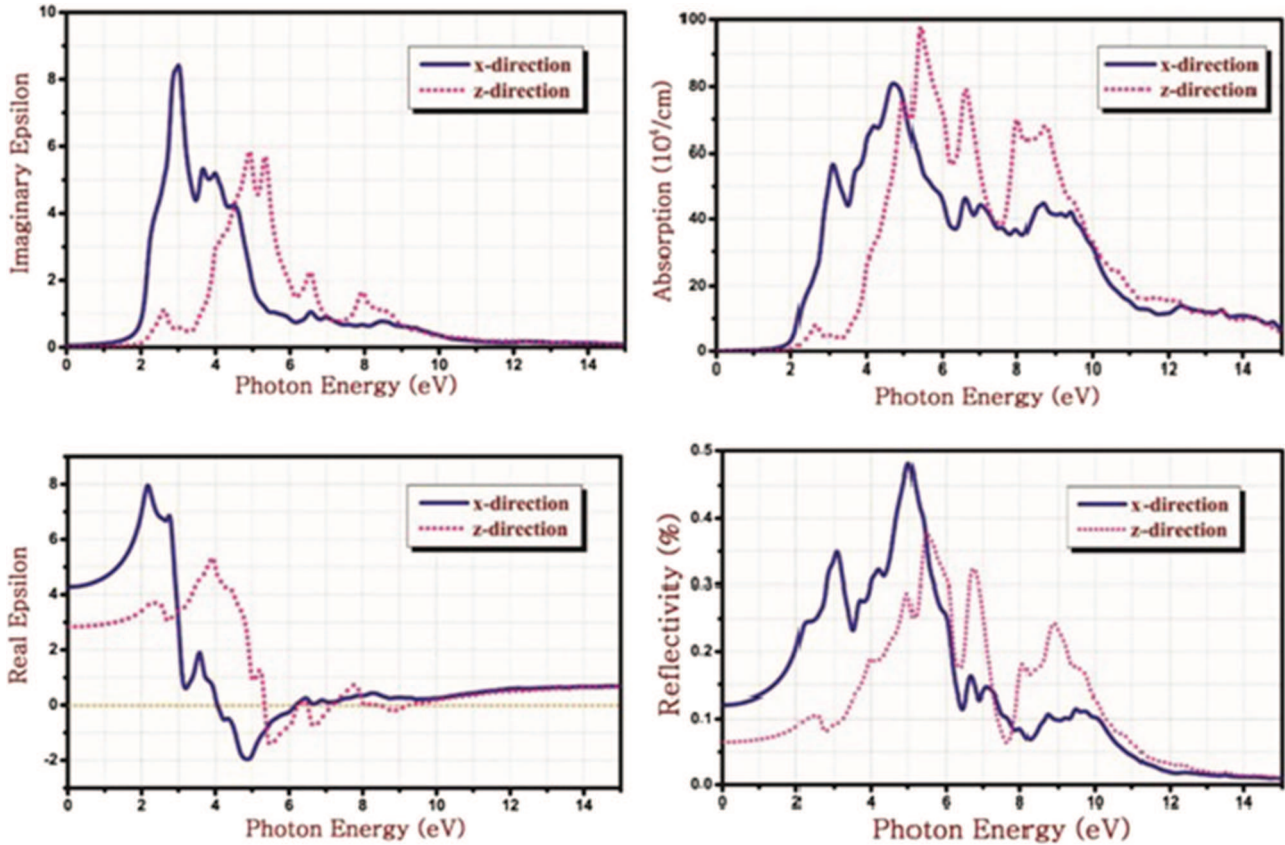
Fig. 5. Real and imaginary parts of the complex dielectric function, and absorption and reflectivity of the 2D **SnTe** monolayer.

in the state density graph represents the location of the Fermi level, which is depicted with a vertical dotted line. The energy gap indicates the conductivity, semiconductivity, and insulating nature of the structure. The total and partial DOS for 2D **SnTe** monolayer is displayed in Figure 4. This figure reveals that both the VBM and CBM of the monolayer are primarily formed by p orbitals of tellurium and tin atoms. However, it is observed that tellurium atoms contribute slightly more to both VBM and CBM states.

In the next step, to learn more about potential optical applications of this monolayer, we investigated its optical behavior. As is known, the optical response of a material to electromagnetic radiation is expressed by the dielectric function, which is a complex function and represented by $\varepsilon(\omega) = \varepsilon_1(\omega) + i\varepsilon_2(\omega)$ at a given frequency. For analyzing the complex optical characteristics of the considered material, Kramer–Kronig transforms need to be used. This approach allows us to determine the real part of the optical dielectric function with the help of its imaginary part. Knowledge of the complex dielectric constant function gives information on the other optical properties of a material, such as reflectivity and absorption coefficients, refractive index, and energy loss function. The reflectivity coefficient is calculated as follows:

$$R(\omega) = \frac{(n-1)^2 + k^2}{(n+1)^2 + k^2}$$

where n and k are the complex refractive index, given by

$$n(\omega) = \sqrt{\frac{(\varepsilon_1^2 + \varepsilon_2^2)^{1/2} + \varepsilon_1}{2}}$$

$$k(\omega) = \sqrt{\frac{(\varepsilon_1^2 + \varepsilon_2^2)^{\frac{1}{2}} - \varepsilon_1}{2}}.$$

The absorption coefficient $\alpha(\omega)$ is obtained using the real and imaginary parts of the complex dielectric function as follows:

$$\alpha(\omega) = \sqrt{2}\omega\left([\varepsilon_1^2 + \varepsilon_2^2]^2 - \varepsilon_1\right)^{1/2}.$$

Here, the corresponding diagrams for the ground state of 2D **SnTe** monolayer are presented in Figure 5. As seen in this figure, **SnTe** monolayer exhibits almost no absorption nor reflectivity in the low-energy and visible regions of the electromagnetic spectrum. However, it is evident from Figure 5 that this 2D monolayer material exhibits good absorption and considerable reflectivity in the ultraviolet (UV) region of the electromagnetic spectrum, suggesting its application in UV shielding technologies.

Analysis of the strain effect on the electronic characteristics of materials is an effective tool for designing electronic structures using 2D materials [43,44]. Therefore, we checked the effect of biaxial strain on the electronic and
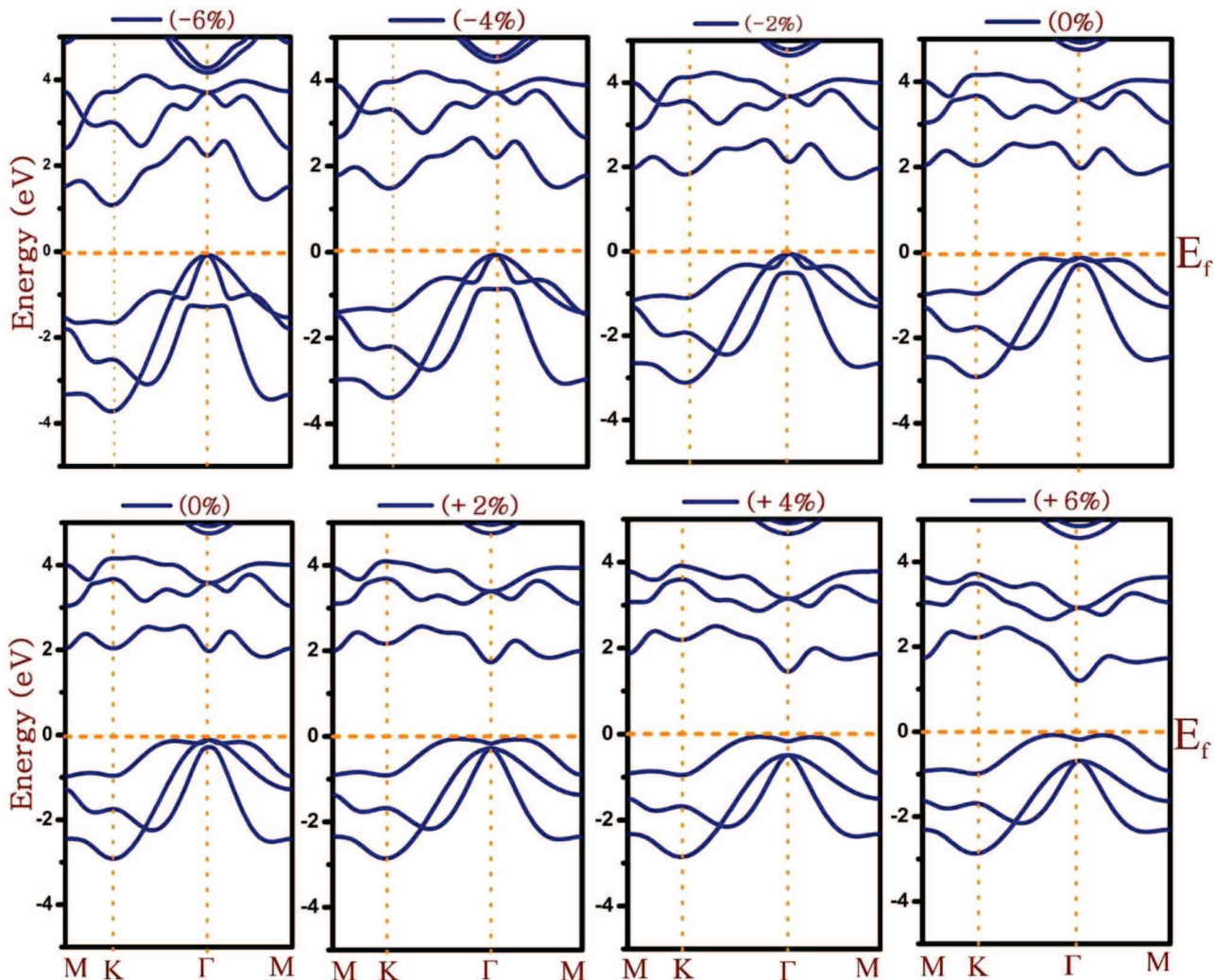
Fig. 6. Band structures of all strain states of **SnTe** calculated by using the GGA PBE approximation.

Table 1. Structural properties and electronic band gaps of 2D **SnTe** monolayer under strain conditions (obtained by using PBE theory).

Strain value (%)	−6	−4	−2	0	2	4	6
a = b (Å)	3.955	4.041	4.123	4.207	4.291	4.375	4.46
Gap (eV)	1.245	1.622	1.844	2.000	1.914	1.664	1.413
ES (eV/atom)	0.006	0.0034	0.0013	0.000	0.00046	0.001685	0.00332
Δ Sn-Te (Å)	1.776	1.739	1.705	1.678	1.638	1.604	1.567

optical properties of 2D **SnTe** monolayer. Under strain conditions, we calculated the band structure as well as the absorption and reflectivity of the monolayer. In our computation, the strain value is referred to the variation of the lattice constants under stress and is defined by $a = a_0 (1 + \varepsilon)$, where a_0 and a are the strained and unstrained lattice constants, respectively. The following strains are considered: $\varepsilon = 0\%$, $\pm 2\%$, $\pm 4\%$, and $\pm 6\%$, where the positive and negative values correspond to tensile and compressive strains, respectively.

The band structures of **SnTe** monolayer, under different strain conditions, are illustrated in Figure 6. It is evident from this figure that increasing the strain value causes the band gap to decrease under both tensile and compressive strain conditions. Moreover, the curvature of the band structure increases under compressive strains ($\varepsilon < 0$); i.e., the material has higher carrier mobility and conductivity. However, because 2D **SnTe** monolayer is a strain-sensitive material, it has good potential application in mechanical sensor design. Furthermore, there is variation in the band gap and strain energy ($E_s = (E - E_0)/n$) of the monolayer given in Figure 7. Consideration of the strain energy curve in Figure 7 confirms that the proposed 2D material is fully relaxed and optimized.
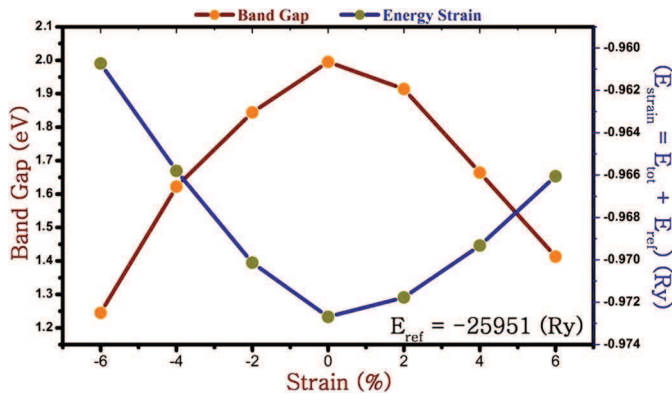
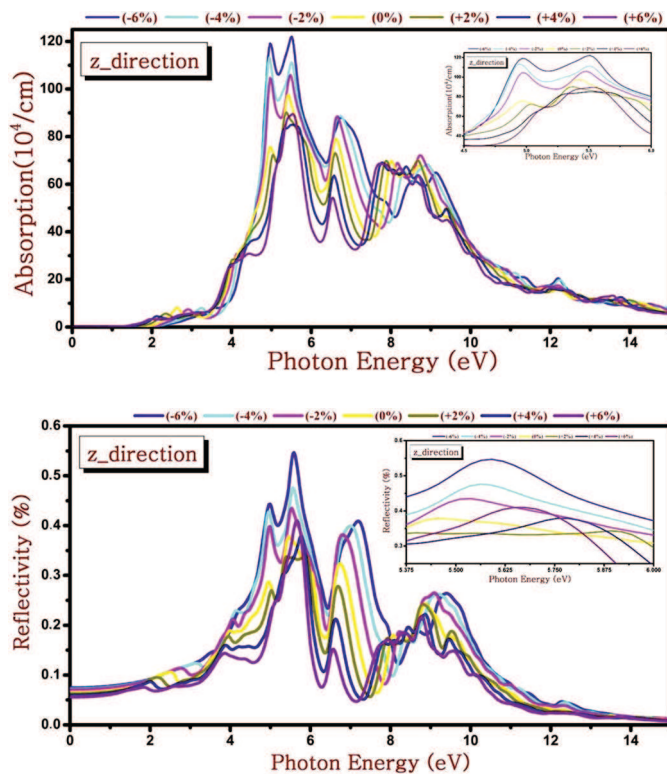**Fig. 7.** Variation of the strain energy gap and energy strain for **SnTe** monolayer.

Fig. 8. Absorption and reflectivity of **SnTe** monolayer for all strain states.

The variation of structural and electronic properties of 2D SnTe monolayer is presented in Table 1.

Finally, in Figure 8 the evolutions of the optical absorption and reflectivity spectra of 2D **SnTe** monolayer are plotted. Close inspection of Figure 8 illustrates that under compressive and tensile strain conditions, the strain value increases, but the absorption and reflectivity coefficients decrease slightly. A blue shift appears in both absorption and reflectivity curves. This optical behavior suggests that use of 2D **SnTe** monolayer in optical devices has potential applications.

5 Conclusions

In summary, the stability and electronic and optical properties of 2D **SnTe** monolayer are studied by using a first-principles calculation in the framework of DFT. According to the calculations, it can be concluded that the predicted 2D **SnTe** monolayer is a stable quasi-direct semiconductor as its stability is proved by cohesive energy calculations and phonon mode analysis. Investigation of the electronic properties of 2D **SnTe** monolayer indicate that this monolayer has a quasi-direct medium band gap of ∼2.00 eV (as calculated by using PBE theory) and ∼2.60 eV (as calculated from HSE06). Therefore, this band gap can be effectively engineered under strain. From the reported results, it can be concluded that the proposed 2D **SnTe** monolayer is a suitable material for designing new optoelectronic devices.

Author contribution statement

Negin Fatahi, Shirin Amirian: carried out the calculations; D. M. Hoat, Amel Laref, A.H. Reshake, Mosayeb Naseri: developed the theory and calculations. All authors analyzed and discussed the results, and contributed to the final manuscript.

References

1. B. Smiri, I. Fraj, M. Bouzidi, F. Saidi, A. Rebey, H. Maaref, Results Phys. **12**, 2175 (2019)
2. D. Chen, G. Zhang, Z. Cheng, S. Dong, Y. Wang, IUCrJ **6**, 189 (2019)
3. K.S. Novoselov, A.K. Geim, S.V. Morozov, D. Jiang, Y. Zhang, S.V. Dubonos, I.V. Grigorieva, A.A. Firsov, Science **306**, 5696 (2004)
4. A.K. Geim, K.S. Novoselov, Nat. Mater. **6**, 183 (2007)
5. X. Zhang, Y. Xie, Chem. Soc. Rev. **42**, 8187 (2013)
6. Q. Tang, Z. Zhou, Prog. Mater. Sci. **58**, 1244 (2013)
7. K.J. Koski, Y. Cui, ACS Nano **7**, 3739 (2013)
8. L. Chen, C.C. Liu, B. Feng, X. He, P. Cheng, Z. Ding, S. Meng, Y. Yao, K. Wu, Phys. Rev. Lett. **109**, 056804 (2012)
9. A.L. Ivanovskii, A.N. Enyashin, Russ. Chem. Rev. **82**, 735 (2013)
10. M. Naguib, V.N. Mochalin, M.W. Barsoum, Y. Gogotsi, Adv. Mater. **26**, 992 (2014)
11. P.Z. Tang, P.C. Chen, W.D. Cao, H.Q. Huang, S. Cahangirov, L.D. Xian, Y. Xu, S.C. Zhang, W.H. Duan, A. Rubio, Phys. Rev. B **90**, 121408 (2014)
12. P. Vogt, P. De Padova, C. Quaresima, J. Avila, E. Frantzeskakis, M.C. Asensio, A. Resta, B. Ealet, G. Le Lay, Phys. Rev. Lett. **108**, 155501 (2012)
13. S. Cahangirov, M. Topsakal, E. Akturk, H. Sahin, S. Ciraci, Phys. Rev. Lett. **102**, 236804 (2009)
14. H. Lu, S-D. Li, J. Mater. Chem. C **1**, 3677 (2013)
15. P. Vogt, P. De Padova, C. Quaresima, J. Avila, E. Frantzeskakis, M.C. Asensio, A. Resta, B. Ealet, G. Le Lay, Phys. Rev. Lett. **108**, 155501 (2012)
16. M.E. Dávila, L. Xian, S. Cahangirov, A. Rubio, G. Le Lay, New J. Phys. **16**, 095002 (2014)

17. S. Balendhran, S. Walia, H. Nili, S. Sriram, Small **11**, 640 (2014)
18. S. Zhang, M. Xie, F. Li, Z. Yan, Y. Li, E. Kan, W. Liu, Z. Chen, H. Zeng, Angew. Chem. Int. Ed. **55**, 1666 (2016)
19. M. Xie, S. Zhang, B. Cai, Y. Huang, Y. Zou, B. Guo, Y. Gu, H. Zeng, Nano Energy **28**, 433 (2016)
20. X. Yu, S. Zhang, H. Zeng, Q.J. Wang, Nano Energy **25**, 34 (2015)
21. S. Zhang, Z. Yan, Y. Li, Z. Chen, H. Zeng, Angew. Chem. Int. Ed. **54**, 3112 (2015)
22. J. Ji, J. Liu, Z. Yan, C. Huo, S. Zhang, M. Su, L. Liao, W. Wang, Z. Ni, Y. Hao, H. Zeng, Nat. Commun. **7**, 13352 (2016)
23. S. Zhang, J. Zhou, Q. Wang, X. Chen, Y. Kawazoe, P. Jena, Proc. Natl. Acad. Sci. **112**, 2372 (2015)
24. A. Lopez-Bezanilla, P.B. Littlewood, J. Phys. Chem. C. **119**, 19469 (2015)
25. S. Zhang, J. Zhou, Q. Wang, P. Jena, J. Phys. Chem. C. **120**, 3993 (2016)
26. F. Li, K. Tu, H. Zhang, Z. Chen, Phys. Chem. Chem. Phys. **17**, 24151 (2015)
27. F. Li, K. Tu, H. Zhang, Z. Chen, Phys. Chem. Chem. Phys. **17**, 24151 (2015)
28. M. Naseri, Appl. Surf. Sci. **423**, 566 (2017)
29. M. Naseri, S. Lin, J. Jalilian, J. Gu, Z. Chen, Front. Phys. **13**, 138102 (2018)
30. M. Naseri, Chem. Phys. Lett. **685**, 310 (2017)
31. H. Morshedi, M. Naseri, M.R. Hantehzadeh, S.M. Elahi, J. Electron. Mater. **47**, 2290 (2018)
32. M. Naseri, Phys. Lett. A **382**, 710 (2018)
33. M. Naseri, Chem. Phys. Lett. **706**, 99 (2018)
34. D. Wang, Y. Wu, Z. Wan, F. Wang, Z. Wang, C. Hu, X. Wang, H. Zhou, RSC Adv. **9**, 19495 (2019)
35. J. Qin, C. Hao, D. Wang, F. Wang, X. Yan, Y. Zhong, Z. Wang, C. Hu, X. Wang, J. Adv. Res. **21**, 25 (2020)
36. P. Blaha, K. Schwarz, G. Madsen, D. Kvasnicka, J. Luitz, K. Schwarz, *WIEN2k Users Guide: An Augmented Planewave+Local Orbitals Program for Calculating Crystal Properties*, Revised Edition WIEN2k 13.1 (Austria, Vienna University of Technology, 2013)
37. J.P. Perdew, K. Burke, M. Ernzerhof, Phys. Rev. Lett. **77**, 3865 (1996)
38. J. Heyd, G.E. Scuseria, M. Ernzerhof, J. Chem. Phys. **121**, 1187 (2004)
39. H.J. Monkhorst, J.D. Pack, Phys. Rev. B **13**, 5188 (1976)
40. P. Giannozzi, S. Baroni, N. Bonini, M. Calandra, R. Car, C. Cavazzoni, D. Ceresoli, G.L. Chiarotti, M. Cococcioni, I. Dabo, J. Phys: Condens. Matter **21**, 395502 (2009)
41. N. Troullier, J.L. Martins, Phys. Rev. B **43**, 1993 (1991)
42. F. Birch, J. Geophys. Res. B **91**, 4949 (1986)
43. M. Naseri, J. Jalilian, Mater. Res. Bull. **88**, 49 (2017)
44. M. Naseri, J. Jalilian, F. Parandin, K. Salehi, Phys. Lett. A **382**, 2144 (2018)